Eur. Phys. J. A (2017) **53**: 50
DOI 10.1140/epja/i2017-12224-7

THE EUROPEAN PHYSICAL JOURNAL A

Regular Article – Experimental Physics

Shell evolution of stable N = 50–56 Zr and Mo nuclei with respect to low-lying octupole excitations

E.T. Gregor[1,2,a], M. Scheck[1,2,b], R. Chapman[1,2], L.P. Gaffney[1,2], J. Keatings[1,2], K.R. Mashtakov[1,2], D. O'Donnell[1,2], J.F. Smith[1,2], P. Spagnoletti[1,2], M. Thürauf[3], V. Werner[3], and C. Wiseman[1,2]

[1] School of Engineering and Computing, University of the West of Scotland, Paisley, PA1 2BE, UK
[2] SUPA, Scottish Universities Physics Alliance, Glasgow G12 8QQ, UK
[3] Institut für Kernphysik, Technische Universität Darmstadt, D-64289 Darmstadt, Germany

Received: 22 November 2016 / Revised: 19 January 2017
Published online: 15 March 2017

Communicated by N. Kalantar-Nayestanaki

Abstract. For the $N = 50$–56 zirconium ($Z = 40$) and molybdenum ($Z = 42$) isotopes, the evolution of subshells is evaluated by extracting the effective single-particle energies from available particle-transfer data. The extracted systematic evolution of neutron subshells and the systematics of the excitation energy of the octupole phonons provide evidence for type-II shape coexistence in the Zr isotopes. Employing a simplistic approach, the relative effective single-particle energies are used to estimate whether the formation of low-lying octupole-isovector excitations is possible at the proposed energies. The results raise doubts about this assignment.

1 Introduction

One of the most fascinating aspects of the nuclear many-body system is the presence of collective excitations at low energies. Since these excitations emerge in a bound quantum system, which necessarily develops a shell structure, it is of interest to understand how these collective excitations evolve in the framework of the single-particle orbits of the shell structure and the residual interactions. Particularly interesting is the formation of collective excitations in nuclei with only a low number of valence particles and even more so when the two-component nature of the nucleus plays a role.

The two-component nature of the nucleus allows for an in-phase and an out-of-phase coupling of proton and neutron subsystems [1]. In the proton-neutron version of the interacting boson approximation (IBA-2) [2], as well as in a schematic shell-model approach [3], it is shown that the first excited 2_1^+ state indeed corresponds to an in-phase excitation of proton and neutron components, which is invariant (isoscalar) under the exchange of proton and neutrons. In contrast, the out-of-phase motion is represented by a wave function which is not symmetric under exchange of protons and neutrons (isovector). Since the proton-neutron interaction is attractive, the symmetric coupling will be shifted to lower energy and the antisymmetric solution to higher energy. A necessary condition for the formation of an isovector state is that both subsystems have at least one basis state in the energy range between the isoscalar and isovector state. Due to their first prediction within the sd-IBM-2 extension of the IBA [2] (where the 2 represents the separate treatment of proton and neutron excitations), this class of states is commonly referred to as mixed-symmetry (ms) states. Since their first observation [4–6] in the 1980s for the quadrupole degree of freedom, a large data basis for low-lying isovector excitations has been established [7–9].

One of the most interesting regions of the nuclear landscape is located around the $Z = 40$ subshell closure and extending from the $N = 50$ shell closure to the $N = 56$ subshell closure. In the valence space of these nuclei, pronounced subshell gaps between the proton (π) $\pi 2p_{3/2^-}, \pi 1f_{5/2^-}$, $\pi 2p_{1/2^-}$ subshells and the isolated $\pi 1g_{9/2^+}$ subshell and between the neutron (ν) $\nu 2d_{3/2^+}$, $\nu 3s_{1/2^+}$, $\nu 1g_{7/2^+}$, $\nu 1h_{11/2^-}$ subshells and the $\nu 2d_{5/2}$ subshell are noticeable. These special shell structures allow for the observation of a variety of very particular behaviours such as a relatively weak, just emerging quadrupole collectivity but a pronounced octupole collectivity and features associated with shape coexistence [10].

The low degree of quadrupole collectivity in the ground-state configuration of the Zr isotopes expresses itself in a comparably high excitation energy of the first

[a] e-mail: e.t.gregor@uws.ac.uk
[b] e-mail: marcus.scheck@uws.ac.uk

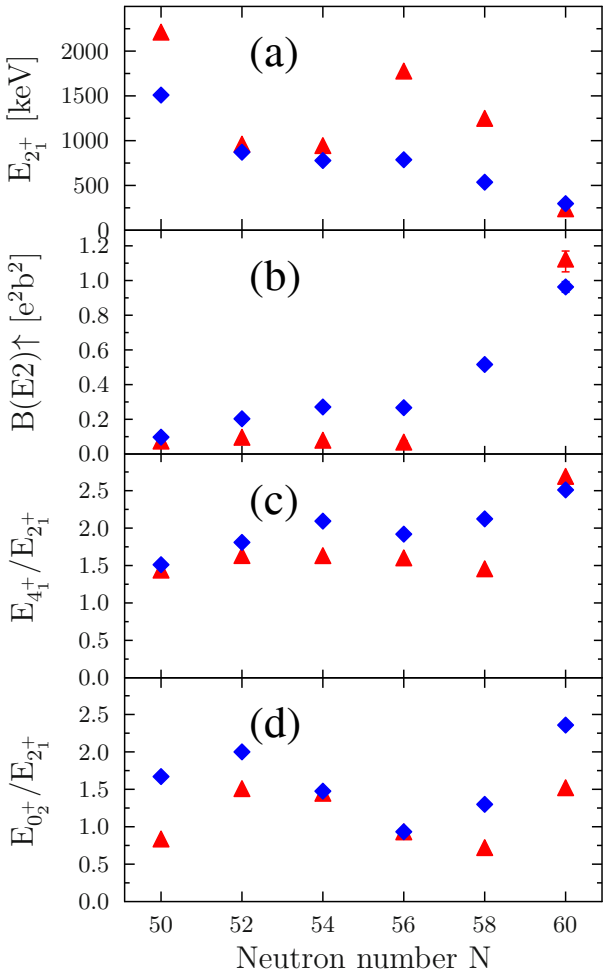

Fig. 1. Quantities highlighting the evolution of quadrupole collectivity in the $N = 50$ to $N = 60$ Zr (red triangles) and Mo (blue diamonds) isotopes. Shown are the excitation energies of the first excited 2_1^+ levels (a), the $B(E2, 0_1^+ \rightarrow 2_1^+)$ excitation strengths (b), the ratio of the excitation energies of the first 4_1^+ and 2_1^+ levels (c), and the ratio of the excitation energies of the first excited 0_2^+ and 2_1^+ levels (d). The data have been taken from refs. [11–13]. For a discussion see text.

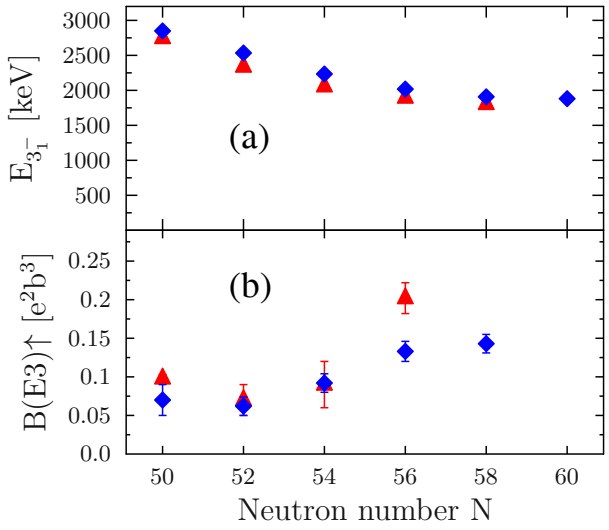

Fig. 2. Quantities highlighting the evolution of octupole collectivity in the $N = 50$ to $N = 60$ Zr (red triangles) and Mo (blue diamonds) isotopes. Shown are the excitation energies of the first excited 3_1^- levels (a), the $B(E3, 0_1^+ \rightarrow 3_1^-)$ excitations strength (b). The data has been taken from refs. [12, 13, 21]. For a discussion see text.

excited 2_1^+ states (fig. 1(a)), low $B(E2, 0_{gs}^+ \rightarrow 2_1^+)$ excitation probabilities (fig. 1(b)) [11], and low $E(4_1^+)/E(2_1^+)$ ratios (fig. 1(c)) [12, 13]. Especially for the Zr isotopes ($Z = 40$) of interest, the $E(4_1^+)/E(2_1^+)$ values well below two indicate a seniority-two scheme rather than a collective pattern. In contrast, for the Mo isotopes ($Z = 42$) these observables indicate a noticeable quadrupole collectivity as the neutron number is increased. The measured g-factors confirm for ^{92,94}Zr [14] a neutron dominance in the 2_1^+ and 4_1^+ states, while the g-factor for the 2_1^+ level in ^{96}Zr [15] exhibits sizeable proton components. The g-factors for the 2_1^+ states of the Mo isotopes [16] exhibit proton contributions in the wave function. Additionally, the energy of the low-lying 0_2^+ levels and in some cases even below the 2_1^+ level, far below the vibrational value of $E_{0_2^+}/E_{2_1^+} \approx 2$, indicates shape or at least configuration coexistence (fig. 1(d)). For several of the nuclei under consideration the structures built upon this low-lying 0^+ level have been shown to possess an enhanced quadrupole collectivity [17–20].

Contrary to the quadrupole collectivity, the octupole collectivity [21] is comparably strong in these nuclei. Especially in the Zr isotopes, phonons of this type are located at, for this mass region, low excitation energies (fig. 2(a)) and exhibit pronounced $B(E3, 0_{gs}^+ \rightarrow 3_1^-)$ excitation probabilities (fig. 2(b)). Interestingly, apart from ^{96}Zr, the trend of the octupole collectivity in the two isotopic chains behaves quite similarly. The slightly lesser collectivity for the Mo isotopes can be explained with blocking of configurations due to the presence of two valence protons in the $\pi 1g_{9/2}$ subshell. The $B(E3)$ reduced transition probability in ^{96}Zr is remarkable. In fact, for ^{96}Zr the currently accepted value of 53(6) W.u. $E3$ strength exceeds the 42(3) W.u. in ^{224}Ra [22] and is comparable to the value of 54(3) W.u. for ^{226}Ra [23]; nuclei for which octupole correlations in the ground state are attributed.

Neglecting excitations across major oscillator shell gaps and two-particle two-hole and four-particle/four-quasiparticle excitations, the octupole collectivity in the vicinity of ^{96}Zr is associated with four configurations, namely the proton $\pi[1g_{9/2^+}, 2p_{3/2^-}^{-1}]_{3^-}$ and $\pi[1g_{9/2^+}, 1f_{5/2^-}^{-1}]_{3^-}$ one-particle one-hole (1p1h) excitations and the neutron $\nu[1h_{11/2^-}, 2d_{5/2^+}]_{3^-}$ and $\nu[1h_{11/2^-}, 1g_{7/2^+}]_{3^-}$ two-particle (2p) excitations. In a simplistic approach, the residual octupole-octupole interaction mixes these configurations to the collective states. The amplitudes of the individual components in the wave function of the resulting 3^- states depend on their relative position

Table 1. Excitation energies of the first 3^-_1 states and of the candidates for low-lying octupole isovector (mixed-symmetry) excitations in Zr and Mo isotopes [25,27].

Nucleus	$E_{3^-_1}$ [keV]	$E_{3^-_{iv}}$ [keV]
^{92}Zr	2340	3450[a]
^{94}Mo	2533	3012
^{96}Mo	2234	3179

[a] In comparison to [25] revised based on (p,p') data [28]. For discussion see text.

as well as on the occupation of the contributing subshells. In particular, the two $\Delta l = 3$ and $\Delta j = 3$ configurations are expected to contribute strongly to the isoscalar octupole phonon [24].

In a recent development, first candidates for low-lying octupole isovector excitations were proposed for some of these Zr and Mo isotopes [25]. Examples in the mass region of interest are shown in table 1. This assignment was based on observed strong $M1$ transitions from higher-lying 3^- levels to the first octupole phonon. Meanwhile, for ^{96}Ru a similar $3^-_2 \rightarrow 3^-_1$ $M1$ transition was observed [26]. In the quadrupole sector, such strong $M1$ transitions to the first 2^+_1 quadrupole phonon in combination with a weakly collective $E2$ ground-state decay serve as the experimental signature of a low-lying isovector (mixed-symmetry) excitation. Furthermore, in particle-scattering experiments such as (p,p') or (e,e') enhanced excitation cross sections are observed for the quadrupole isovector levels, as well as for the octupole isovector candidates. This was seen as additional evidence for the one-phonon character of the proposed isovector octupole excitations [27]. In fact the enhanced excitation cross section in (p,p') experiments [28,29] led for ^{92}Zr to a revision of the candidate for the octupole isovector candidate. The level at 3039 keV, which was proposed in ref. [25] as a candidate, was not observed. This non-observation indicates a non-natural spin and parity of $J^\pi = 3^+$. Instead, a 3^- level at 3446(20) keV exhibits a comparably strong link to the ground state. This is in good agreement with previous particle scattering measurements establishing a 3^- level at 3446 keV [30–32]. In a $(n,n'\gamma)$ measurement [33], a level at 3452.1(3) keV exhibited a link to the first 3^- level. In the $(n,n'\gamma)$ work, spin and parity (2^+) were tentatively assigned but the (p,p') measurement unambiguously assigned 3^-. For ^{94}Zr, the (p,p') data reveal an enhanced excitation cross section for a 3^- state at 3232(10) keV. Similarly, the candidates in ^{94}Mo and ^{96}Mo exhibited strong excitation cross sections.

The aim of this publication is to extract the excitation energies of the valence shell two-body excitations, which contribute to low-lying octupole excitations, and evaluate their evolution as a function of proton and neutron numbers. A further goal is to test whether the proposed candidates for low-lying octupole isovector excitations in the Mo and Zr region fulfill the condition that at least one of the unperturbed 1p1h or 2p/two-quasiparticle excitations for each subsystem must be situated between the energies of the isoscalar 3^-_1 and isovector 3^-_{iv} one-phonon excitations. If this is not the case, an alternative mechanism for the observed $3^-_i \rightarrow 3^-_1$ $M1$ transition strength and the considerable $B(E3)$ excitation strength of these higher-lying excited 3^-_i levels has to be found. As a first step, experimental values of excitation energies of the spherical shell-model orbits are extracted from published particle-transfer experiments and the pairing energies from odd-even mass differences. These values are used to determine the energy at which the initial 1p1h or 2p/two-quasiparticle excitations are situated and to test the possibility of the existence of these 3^-_{iv} states at the proposed excitation energies.

Table 2. Extracted effective single-particle energies of the proton subshells in the odd-mass Y and Nb nuclei of interest. The employed data, together with the reactions and the evaluated data sets, are given in tables 7 and 8. For a discussion see text.

Nucleus	$E_{g_{9/2^+}}$ [keV]	$E_{p_{1/2^-}}$ [keV]	$E_{f_{5/2^-}}$ [keV]	$E_{p_{3/2^-}}$ [keV]
^{89}Y	1013	0	−2057	−1658
^{91}Y	550	−559	−1543	−1227
^{93}Y	775	−625	−1164	−1293
^{95}Y	1090	0	−1040	−1334
^{91}Nb	0	−100	−1762	−1508
^{93}Nb	53	−30	−1320	−1072
^{95}Nb	0	−659	−1487	−1089
^{97}Nb	449	−737	−1694	−1421

2 Experimental values

Experimental values of the spherical shell-model single-particle levels were extracted from a variety of particle-transfer experiments listed in the NNDC [12] and XUNDL [13] databases. The used levels and their spectroscopic factors, together with the reactions with which they were measured and the references, are given in tables 7, 8, 9, and 10 in the appendix.

The effective single-particle energies (ESPE) of the respective subshell E_{nl_j} was calculated using the spectroscopic factor S_i, weighted experimental excitation energies E_i for a given spin j:

$$E_{nl_j} = \frac{\sum_i E_i \cdot S_i}{\sum_i S_i} \,. \tag{1}$$

When the level was seen as situated above the Fermi level (particle excitation), the energy entered in eq. (1) was positive and in the case in which the level was recognised as situated below the Fermi level (hole excitation) the energy entered was negative. The results are presented in tables 2 and 3, and figs. 3 and 4.

Since often no errors for the spectroscopic factors are given in the original publications, it is not possible to calculate errors for the extracted ESPEs when using these

Table 3. Extracted effective single-particle energies of the neutron subshells in the odd-mass Zr and Mo nuclei of interest. The employed data, together with the reactions and the evaluated data sets, are given in tables 9 and 10. For a discussion see text.

Nucleus	$E_{d_{5/2^+}}$ [keV]	$E_{s_{1/2^+}}$ [keV]	$E_{g_{7/2^+}}$ [keV]	$E_{d_{3/2^+}}$ [keV]	$E_{h_{11/2^-}}$ [keV]
^{91}Zr	92	1653	3043	2584	2188
^{93}Zr	0	1208	2075	2734	2363
^{95}Zr	0	1381	2132	2215	2797
^{97}Zr	−1399	0	1265	1108	2541
^{93}Mo	218	1682	2427	1634	2435
^{95}Mo	234	1299	1276	2180	1932
^{97}Mo	704	1273	1085	1700	1672
^{99}Mo	−139	69	236	567	688

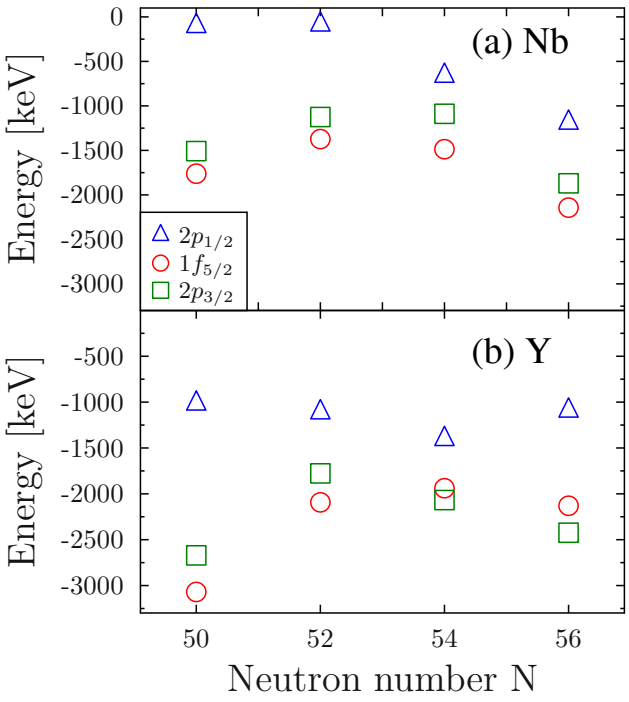

Fig. 3. Effective single-particle energies (ESPE) for the proton subshells for the corresponding Nb (a) and Y (b) isotopes as extracted from published particle-transfer experiments. The energies are normalised relative to the $\pi 1g_{9/2^+}$ subshell ($E_{\pi 1g_{9/2}} = 0$ keV). The numerical values are given in table 2. For a discussion see text and note the different scaling of the y-axes.

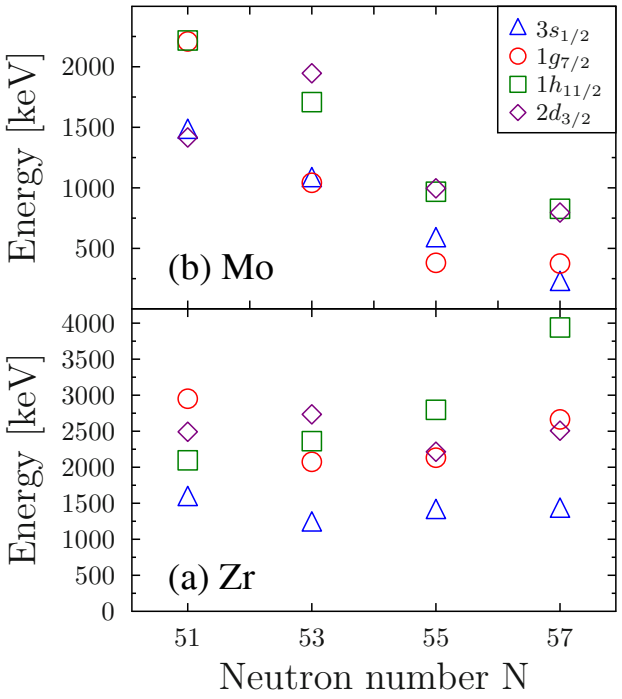

Fig. 4. Effective single-particle energies (ESPE) for the neutron subshells in the Mo (a) and Zr (b) isotopes as extracted from published particle-transfer experiments. The energies are normalised relative to the $\nu 2d_{5/2^+}$ subshell ($E_{\nu 2d_{5/2}} = 0$ keV). The numerical values are given in table 3. For a discussion see text and note the different scaling of the y-axes.

data sets. Besides this systematic uncertainty, there are several ambiguities associated with the extraction of the spherical shells in this work. For the assignments of levels situated near the Fermi level it is not always obvious from the data whether the level corresponds to a particle or a hole excitation. A good example for the influence of these ambiguities is the $\nu 2d_{5/2^+}$ subshell in ^{97}Mo. The spin of a level at 720 keV is not unambiguously determined. It could be $5/2^+$ or $3/2^+$ or even be a doublet. However, if a spin of $3/2^+$ is attributed to this level, the energy of the $\nu 2d_{5/2^+}$ ESPE changes by a negligible amount from 704 keV to 693 keV. The situation is alterated more drastically when a hole character is assigned, then the $\nu 2d_{5/2^+}$ subshell shifts by $\approx$ 500 keV to a lower energy. However, based on the relative spectroscopic factors from the ^{96}Mo(d,p) reaction [34] compared to the ^{98}Mo(p,d) [35] and ^{98}Mo$(\boldsymbol{d},t)$ [36] reactions, a particle character was assigned. This example has been highlighted, because the neutron configurations in ^{97}Mo play a crucial role, in relation to whether the quadrupole collectivity is already enhanced in ^{96}Mo or only in ^{98}Mo. Another ambiguity that is worth mentioning is the situation of the $\pi 1g_{9/2}$ subshell in ^{91}Nb. In the ^{90}Zr(^{3}He,d) reaction [37], besides the ground state, two further levels with an angular-momentum transfer of four were observed. Both levels are showing enhanced spectroscopic factors S; however, their excitation energies of 4817 keV ($S = 2.8$) and 6040 keV ($S = 4.2$) rather qualify them as fragments of the $\pi 1g_{7/2}$ subshell in the next major oscillator shell. The approach of eq. (1) gives a value of 5551 keV for the ESPE of the $\pi 1g_{7/2}$ subshell. This number corresponds to the major shell gap between the proton $N = 3$ and $N = 4$ oscillator shells.

3 Discussion

The evolution of the proton shells is shown in fig. 3, with the ESPE for the $1g_{9/2^+}$ subshell used as a reference ($E_{1g_{9/2}} = 0\,\text{keV}$) and the ESPEs of the other subshells plotted relative to it. The comparison of the results for the proton subshells for the Y ($Z = 39$) and Nb ($Z = 41$) isotopes reveals an enhanced subshell gap for the Y isotopes. Additional support for the reduction of the proton subshell gap, when filling protons in the $\pi 1g_{9/2}$ subshell, is provided by the proton-separation energies. Comparing them for Rb and Y isotopes relative to those of the Nb isotopes supports the assigned gaps for the isotopic chains of interest.

The evolution of a given subshell with changing nucleon number is governed by multiple effects. The two major ones are additional tensor interactions and a change of the spin-orbit interaction. The tensor interaction is attractive between proton-neutron $[j_>, j_<]$ and $[j_<, j_>]$ two-body configurations and repulsive between $[j_<, j_<]$ and $[j_>, j_>]$ combinations. Here, the notation $j_</j_>$ denotes $j_> = l + s/j_< = l - s$ coupling. Consequently, filling neutrons in the $j_> : \nu 2d_{5/2}$ subshell will lower the binding energy of the occupied proton $j_> : \pi 2p_{3/2}$ and $\pi 1g_{9/2}$ subshells, while increasing the binding energy of the $j_< : \pi 2p_{1/2}$ and $\pi 1f_{5/2}$ subshells. For the Mo isotopes, proton occupancy of the $j_> : \pi 1g_{9/2}$ lowers the binding energy of the $j_> : \nu 2d_{5/2}$ subshell, while the latter subshell is gradually being filled. Indeed, while the subshell gap between the $\nu 2d_{5/2}$ and the other neutron subshells stays preserved for the Zr isotopes (fig. 4(a)), for the Mo isotopes (fig. 4(b)) the binding energy of the $\nu 2d_{5/2}$ subshell is lowered. The migration of the $\nu 2d_{5/2}$ subshell towards the other subshells results in a vanishing subshell gap. The second effect is the change of the spin-orbit interaction V_{ls}, which is linked to the shape of the mean-field potential $V(r)$ ($V_{ls} \propto -\partial V(r)/\partial r$). The shrinking of the energy difference of the $\pi 2p_{3/2}$–$\pi 2p_{1/2}$ spin-orbit partners for the Nb isotopes with increasing neutron number indicates a weakening of this force, which will more strongly affect the interaction between the $\pi 1g_{9/2}$ and its $\pi 1g_{7/2}$ spin-orbit partner in the next oscillator shell. Indeed, the binding energy of the $\pi 1g_{9/2}$ subshell in the heavier Nb isotopes is lowered and it migrates away from the other proton subshells. Interestingly, for neutron orbitals in the Zr isotopes, the $\nu 2d_{5/2}$–$\nu 2d_{3/2}$ subshells exhibit a rather constant energy difference, but the unoccupied and, therefore, unaffected by the tensor interaction $\nu 1h_{11/2}$ subshell exhibits a strong lowering in binding energy with increasing neutron number. This shift indicates a variation of the neutron mean-field potential, while the proton subshells in the Y isotopes do not exhibit a variation. For the Mo isotopes no such migration of the $\nu 1h_{11/2}$ subshell is observed, while the $\nu 2d_{5/2}$–$\nu 2d_{3/2}$ splitting is slightly reduced due to the tensor interaction with the two protons in the $\pi 1g_{9/2}$ subshell. Relative to the ESPE of the $\nu 3s_{1/2}$ subshell, which is neither influenced by the tensor nor by the spin-orbit interaction, the ESPE of the $\nu 1h_{11/2}$ subshell is stable. Obviously, the presence of protons in the $\pi 1g_{9/2}$ stabilises the neutron mean-field potential and has a massive effect on the evolution of the neutron subshells in this mass region.

Table 4. Pairing energies for protons Δ_π and neutrons Δ_ν for the given neutron numbers N calculated using experimental masses [39] and eq. (2). The values are given in units of keV.

	N	50	52	54	56	58
Δ_π	Mo	1419	1510	1520	1410	1631
	Zr	1119	1265	1303	1484	1523
Δ_ν	Mo	1791	979	1030	1135	1315
	Zr	1856	836	811	918	713

3.1 Excitation energy of the 1p1h or 2p/two-quasiparticle basis states

In the following, the extracted ESPEs are employed in a calculation of the excitation energies of the four valence space two-body excitations that can contribute to an octupole excitation.

Besides the ESPEs, the second important ingredient to estimate the location of the 1p1h or 2p/two-quasiparticle excitations is the pairing energy Δ_ρ ($\rho = \pi$ or ν). In order to determine this crucial quantity, eqs. (2.92) and (2.93) from ref. [38]:

$$\begin{aligned}\Delta_\nu &= \frac{1}{4}\left[B(N-2,Z) - 3\cdot B(N-1,Z)\right.\\ &\quad \left. + 3\cdot B(N,Z) - B(N+1,Z)\right],\\ \Delta_\pi &= \frac{1}{4}\left[B(N,Z-2) - 3\cdot B(N,Z-1)\right.\\ &\quad \left. +3\cdot B(N,Z) + B(N,Z+1)\right] \qquad (2)\end{aligned}$$

were employed. The total nuclear binding energies $B(N,Z)$ are extracted from mass measurements [39]. The extracted values of Δ_π and Δ_ν are presented in table 4. Here it should be mentioned that the use of the double mass-difference formula (eq. (2.96) in ref. [38]) results in comparison to eq. (2) in higher pairing energies, by approximately 200 keV for the neutrons and approximately 300 keV for the protons.

3.1.1 Particle-hole picture

In order to evaluate the energetic position $E_{1p1h/2p}$ of the proton 1p1h and neutron 2p configurations for the even-even nuclei, the simple ansatz of

$$\begin{aligned}E_{1p1h} &= \Delta E_{shells} + 2\Delta_\rho,\\ E_{2p} &= \Delta E_{shells,1} + \Delta E_{shells,2} + 2\Delta_\rho \qquad (3)\end{aligned}$$

is made in this section. Here, ΔE_{shells} is the energy difference of the two subshells contributing to the 1p1h or

Table 5. Energies for the 1p1h and 2p/two-quasiparticle excitations of interest. The values were extracted using eq. (3) for the particle-particle and particle-hole picture and eqs. (4) and (5) in the quasi-particle approach. The energies are given in units of keV.

	Neutron number:	50	52	54	56
Mo	$\pi[1g_{9/2}, 2p_{3/2}^{-1}]$	4346/3454	4145/3355	4129/3254	4690/3432
	$\pi[1g_{9/2}, 1f_{5/2}^{-1}]$	4600/3644	4393/3524	4527/3466	4963/3625
	$\nu[1h_{11/2}, 2d_{5/2}]$		3916/3168	3393/2715	3168/2487
	$\nu[1h_{11/2}, 1g_{7/2}]$		5541/4086	4104/2936	3546/2485
Zr	$\pi[1g_{9/2}, 2p_{3/2}^{-1}]$	4909/3665	4307/3140	4674/3368	5392/3975
	$\pi[1g_{9/2}, 1f_{5/2}^{-1}]$	5308/4025	4623/3373	4545/3277	5098/3752
	$\nu[1h_{11/2}, 2d_{5/2}]$		3902/3174	4202/3515	5205/4647
	$\nu[1h_{11/2}, 1g_{7/2}]$		6415/4943	6306/4959	7603/6068

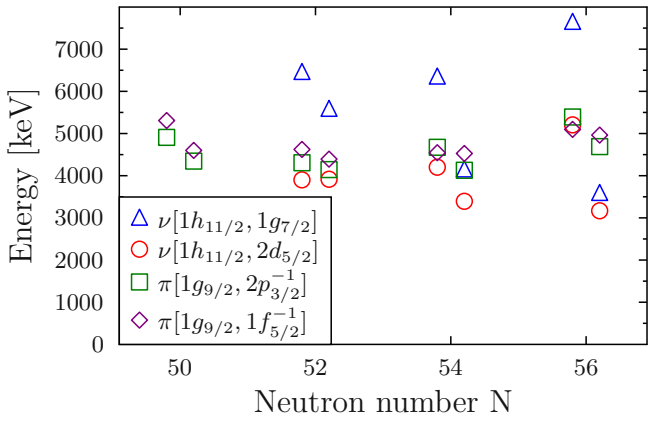

Fig. 5. Excitation energies for the 1p1h or 2p excitations, which can contribute to a valence shell 3^- configuration. The values were calculated using eq. (3). For clarity of the presentation the values for the Zr (Mo) isotopes are slightly shifted to the left (right) of the corresponding neutron number.

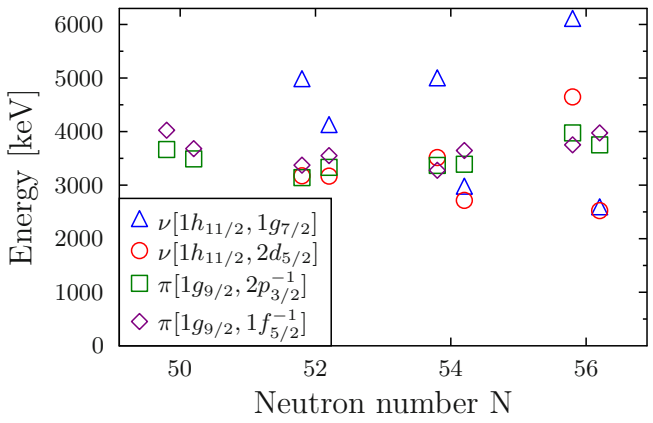

Fig. 6. Excitation energies for the two-quasiparticle configurations, which can contribute to a valence shell 3^- configurations. The values were calculated using eqs. (4) and (5). For clarity of the presentation the values for the Zr (Mo) isotopes are slightly shifted to the left (right) of the corresponding neutron number.

for the 2p excitation it is the energy difference of the two subshells and the subshell containing the Fermi level, and $2\Delta_\rho$ ($\rho = \pi$ or ν) is the pairing energy for protons and neutrons, respectively. Any configuration dependence of the pairing energy is ignored. For the proton configurations of the Zr isotopes the subshell structure of the Y isotopes was used and for the Mo isotopes the subshells of the Nb isotopes were employed as ΔE_{shells}. In order to calculate ΔE_{shells} for the neutrons, the average energy of the ESPE of the given subshell in the two adjacent odd-mass nuclei was used. The results are presented in table 5 and fig. 5. Remarkable is that the proton 1p1h energies are almost equal for the Zr and Mo isotopes with equal neutron number. Obviously, the higher energy of the subshell gap is compensated by a lower pairing energy.

3.1.2 Quasiparticle picture

An alternative approach to extract the basis states exploits the quasiparticle energy E_{qp} [38]:

$$E_{qp} = \sqrt{(E_{nl_j} - \lambda)^2 + \Delta_\rho^2}\,. \tag{4}$$

For the chemical potential λ, a couple of assumptions were made. In the cases where the subshell is not completely filled, the chemical potential is assumed to be situated in this subshell. When the subshell is in the particle picture completely filled the chemical potential was taken as half the difference between the ESPE of the last fully-occupied subshell and the ESPE of the next empty subshell. For example, the chemical potential for protons in the Zr isotopes was taken as half the difference of the ESPE of the $\pi 1g_{9/2}$ and the $\pi 2p_{1/2}$ subshells.

The excitation energy of the two-quasiparticle configuration is calculated as the sum of the two individual quasiparticle energies

$$E_{[qp_i, qp_j]_{J^\pi}} = E_{qp_i} + E_{qp_j}\,. \tag{5}$$

The results for the calculated two-quasiparticle energies are presented in table 5 and shown in fig. 6. Remarkably, for both approaches, the proton 1p1h/two-quasiparticle excitations for the Zr and Mo isotopes

Table 6. Energies for the 1p1h or 2p/two-quasiparticle excitations of the test cases extracted using eq. (3) for the particle-particle and particle-hole picture and eqs. (4) and (5) in the quasiparticle approach. The energies are given in units of keV.

	Neutron number:	50	52	54	56
Zr	$\pi[1g_{9/2}, 2p^{-1}_{1/2}]$	3251/2457	3639/2762	4006/2958	4058/3162
	$\pi[2p^{-1}_{3/2}, 2p^{-1}_{1/2}]$	5922/3665	5416/3140	6074/3368	6482/3975
	$\nu[2d_{5/2}, 2d_{3/2}]$		4290/3540	4101/3419	4197/3689
Mo	$\pi[1g_{9/2}, 2p^{-1}_{1/2}]$	2938/2840	3103/3021	3699/3111	4006/3059
	$\pi[2p^{-1}_{3/2}, 2p^{-1}_{1/2}]$	4446/3454	4228/3355	4788/3254	5876/3432
	$\nu[2d_{5/2}, 2d_{3/2}]$		3639/2924	3531/2826	3121/2463

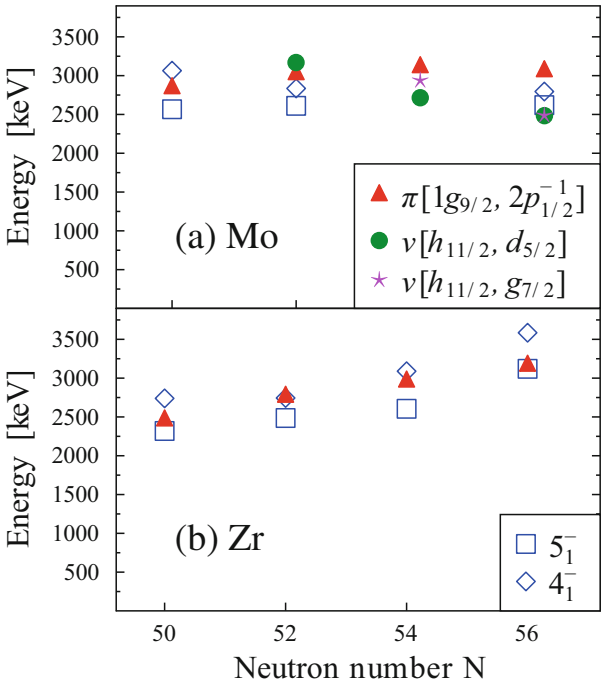

Fig. 7. Excitation energies for the first experimentally observed 4^-_1 (blue open diamond) and 5^-_1 (blue open square) levels [12, 13, 19] and the $\pi[1g_{9/2}, 2p^{-1}_{1/2}]$ two-quasiparticle configuration (red triangle) calculated in this work. Additionally, for the Mo isotopes the $\nu[1h_{11/2}, 2d_{5/2}]$ (green circle) and $\nu[1h_{11/2}, 1g_{7/2}]$ (magenta star) two-quasiparticle configurations are shown. For a discussion see text.

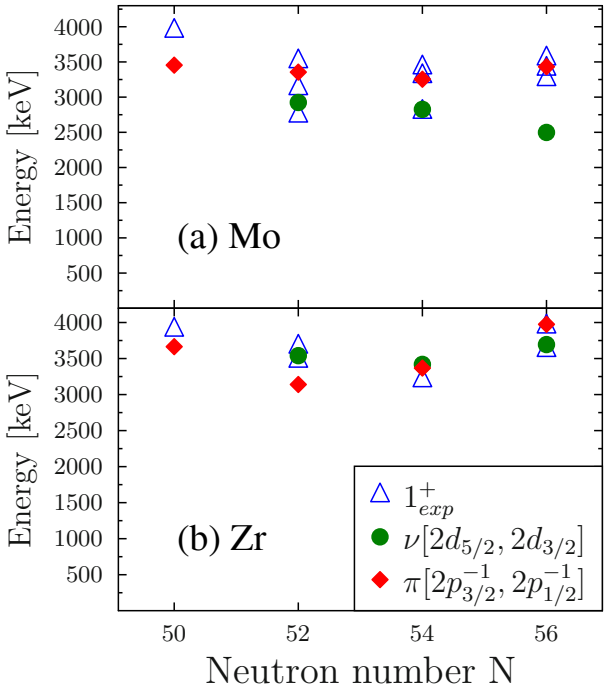

Fig. 8. Excitation energies for the experimentally observed first excited 1^+ levels (blue open triangle) [40–46] and the neutron $[2d_{5/2}, 2d_{3/2}]$ (green circle) and proton $[2p_{3/2}, 2p_{1/2}]$ (red diamond) two-quasiparticle configurations extracted in this work. For a discussion see text.

with equal neutron number are found at approximately the same energy. However, the neutron 2p/two-quasiparticle excitations differ strongly. In comparison to the particle-hole/particle-particle approach, the two-quasiparticle excitations are found at approximately 1 MeV lower energies.

3.1.3 Test cases

In order to test the simple approach used here, the 4^- and 5^- levels resulting from the $\pi[1g_{9/2}, 2p^{-1}_{1/2}]$ coupling and the $\pi[2p^{-1}_{3/2}, 2p^{-1}_{1/2}]$ and $\nu[2d_{3/2}, 2d_{5/2}]$ 1^+ spin-flip excitations are chosen. Additionally for the Mo isotopes the $\nu[1h_{11/2}, 2d_{5/2}]$ and $\nu[1h_{11/2}, 1g_{7/2}]$ configurations are considered. The $\pi[1g_{9/2}, 2p^{-1}_{1/2}]$ coupling as well as the $\nu[1h_{11/2}, 2d_{5/2}]$ and $\nu[1h_{11/2}, 1g_{7/2}]$ configurations (presented in table 5) can be expected in the same energy region (*e.g.*, see ref. [7]). The extracted results are given in table 6 and the experimental values for the low-lying 4^-, 5^-, and 1^+ levels are shown in figs. 7 and 8. Experimental data for the 4^- and 5^- states were taken from the NNDC [12] and XUNDL [13] databases, and ref. [19]. The

data for the 1^+ levels were taken from refs. [40–46]. These test cases indicate that in the particle picture the calculated 1p1h/2p energies are found at considerably higher energy than the experimental levels. In an evaluation of a ^{90}Zr$(n, n'\gamma)$ inelastic neutron-scattering experiment [47], which considered the results of particle-scattering experiments, several of the particle-hole mulitplets were identified. When comparing these results to the extracted values of the particle-hole picture from this study, it is obvious that the values extracted in this study are in general 500–800 keV above the experimental ones. Consequently, the energies for the 1p1h/2p excitations extracted in this approach are rather an upper limit.

However, the two-quasiparticle approach is in good agreement with the experimental data, especially, when considering that pure states are assumed, which is a crude estimation for an open-shell nucleus. Furthermore, the splitting of the $\pi[1g_{9/2}, 2p^{-1}_{1/2}]$ doublet due to residual forces has been neglected [48–51], which results in a slight shift of the experimental values to lower energies. The only exception is ^{98}Mo, for which the calculated energy shift of the neutron two-quasiparticle configurations mismatches the experimental values. This mismatch amounts to 500 keV. Since ^{100}Mo exhibits a noticable degree of quadrupole collectivity, it is likely that the Nilsson splitting sets in and the picture of spherical shells used here is no longer valid. Hence, experimental levels for ^{99}Mo might have been assigned to the wrong subshell and the picture is obscured, resulting in too low-energy differences between the $2d_{5/2}$ and the other subshells. Other possibilities are related to the previously discussed wrong assignment of a hole excitation as a particle excitation or that the employed data sets are missing hole fragments of the $\nu 2d_{5/2}$ subshell. Nevertheless, with the overall satisfactory agreement the two-quasiparticle picture has resulted in its adoption for a further evaluation, which now follows.

4 First excited 3^-_1 levels

Considering the discussed differences of the neutron shell structure for the Mo and Zr isotopes, the similar behaviour of the excitation energy of the first 3^-_1 levels in these isotopic chains (see fig. 2(a)) is quite astonishing, especially when recalling that the $\nu 1h_{11/2}$ subshell, which evolves quite differently in the two isotopic chains, plays a crucial role for this excitation. An explanation is provided by the proposed mechanism of type-II shape coexistence [52], which was already applied to explain features in the quadrupole sector of ^{96}Zr [20]. This mechanism describes the reordering of the subshell structure caused by altered subshell occupancies in excited states. The octupole excitations in the nuclei under consideration here provide further evidence for this mechanism. As previously stated, the octupole excitation in this mass region involves the $\pi[1g_{9/2}, 2p^{-1}_{3/2}]$ and $\pi[1g_{9/2}, 2f^{-1}_{5/2}]$ particle-hole excitations, with a proton excited into the $\pi 1g_{9/2}$ subshell. The assumption, that this partial occupancy is sufficient to reorder the neutron subshell sequence of the Zr isotopes to resemble the one of the Mo isotopes (see fig. 4(b)), provides a natural explanation of the observed trend of the excitation energies of the first 3^-_1 levels. The slightly higher 3^-_1 energies for the Mo isotopes can be explained either with blocking of proton configurations due to the presence of the two protons in the $\pi 1g_{9/2}$ subshell or due to an alteration of the proton subshells due to the occupancy of the neutron $1h_{11/2}$ subshell. Here one has to bear in mind that a collective octupole excitation also includes the $\nu[1h_{11/2}, 2d_{5/2}]$ and $\nu[1h_{11/2}, 1g_{7/2}]$ excitations. Analoguously to the previous argument, the neutron partially occupying the $1h_{11/2}$ subshell will reduce the binding energy of the $j_>\pi 1g_{9/2}$ subshell via the tensor interaction. This effect should be stronger for the Mo isotopes, in which the two protons permanently occupy the $\pi 1g_{9/2}$ subshell, as compared to the Zr isotopes, for which the $\pi 1g_{9/2}$ subshell is only partially occupied in the excited state. Unfortunately, the presented data offer no opportunity to investigate the influence of neutrons in the $\nu 1h_{11/2}$ subshell on the sequence of the proton subshells. This very interesting point is beyond the reach of this study and can only be clarified in a theoretical investigation.

As shown in fig. 6 the $\pi[1g_{9/2}, 2p^{-1}_{3/2}]$ and $\pi[1g_{9/2}, 2f^{-1}_{5/2}]$ proton two-quasiparticle energies are similar for the two isotopic chains and stay almost constant, so that the lowering of the energy at which the isoscalar octupole phonon is observed, when adding neutrons, can be attributed to the lowering of the neutron $\nu[1h_{11/2}, 2d_{5/2}]$ and $\nu[1h_{11/2}, 1g_{7/2}]$ configurations in the Mo isotopes. Indeed, for the Zr isotopes the M_ν/M_π ratio of the neutron multipole transition density M_ν and of the proton multipole transition density M_π for the 3^-_1 levels as extracted from α-scattering experiments [53] exhibits an increase of M_ν and is indicative of stronger neutron components in the neutron richer isotopes. However, the authors of this reference state in the relation to the uncertainties in their model-dependent analysis that not too much weight should be put on their results. Furthermore, some of the $B(E3)$ values the authors used are too low in comparison to the currently accepted values [21], which do reduce the M_ν/M_π ratio. The latter is particularly true for ^{96}Zr; the authors give an additional result for a $B(E3)$ value slightly lower than the currently accepted value resulting in a slight proton dominance. The measured g-factor of $g(3^-_1) = +0.98(15)$ [15] seems to confirm the proton dominance of the 3^-_1 wave function in ^{96}Zr but the g-factor of the $\nu[1h_{11/2}, 2d_{5/2}]$ configration is calculated to be close to zero and the neutron contribution cannot be quantified.

Concerning the neglected excitations across major shell gaps, a recent theoretical investigation [54] of the quadrupole collectivity in the Zr isotopes has shown the importance of higher-lying configurations outside the valence space in order to describe the observed excitation strengths. With respect to the octupole degree of freedom, the importance of such configurations is known from the comparably strong $B(E3, 0^+ \rightarrow 3^-_1)$ value of the doubly magic nucleus ^{208}Pb [21], for which the 3^-_1 level is the first excited state at 2614 keV. The importance of these config-

urations is underlined by the first 3^-_1 in ^{90}Zr. In this semi-magic nucleus the levels with a dominant $[1g_{9/2}, 1f^{-1}_{5/2}]$ and $[1g_{9/2}, 2p^{-1}_{3/2}]$ configurations are identified at 4495 keV and 4536 keV, respectively. These configurations will be strongly involved in the formation of the 3^-_1 level and have comparably large amplitudes but the wave function contains also a vast number of other configurations, in particular, 1p1h across the $N = 50$ and $Z = 50$ shell gaps. Consequently, if one is to understand the behaviour of the $B(E3, 0^+ \rightarrow 3^-_1)$ strength, these configurations must be accounted for, which is beyond the capabilitites of this study.

5 Candidates for low-lying octupole isovector states

As previously stated, the necessary condition for the formation of an isovector state is that both subsystems have at least one basis state between the energy of the 3^-_1 isoscalar excitation and the 3^-_{iv} isovector candidate. The extracted energies of the 1p1h or 2p/two-quasiparticle excitations are summarised in table 5. In the particle-hole picture (see fig. 5) this condition is not fulfilled for any of the candidates. The results of the quasiparticle approach are shown in fig. 6. With respect to the formation of low-lying octupole isovector states, the extracted two-quasiparticle energies raise doubts concerning the nature of the assigned candidates in the two Mo isotopes. The proton two-quasiparticle excitations are found at too high an energy. However, within the previously mentioned uncertainties, for ^{92}Zr the $\Delta l = \Delta j = 3$ octupole driving $\pi[1g_{9/2}, 2p^{-1}_{3/2}]$ and $\nu[1h_{11/2}, 2d_{5/2}]$ two-quasiparticle energies are situated within the energies of the isoscalar 3^-_1 octupole phonon ($E_{3^-_1} = 2340$ keV) and the revised isovector-octupole candidate ($E_{3^-_{iv}} = 3450$ keV). Nevertheless, their energy is relatively close to the excitation energy of the 3^-_{iv} candidate. This finding raises doubts whether the proposed candidates can be an isovector state. If an isovector nature can be attributed, it might be rather a fragment of this state mixed into a 3^- level with another structure. One should also bear in mind, that, as previously pointed out, the extracted ESPEs and, therefore, two-quasiparticle energies are rather lower limits associated with large uncertainties.

One possibility for an alternative interpretation of the nature of these levels has been highlighted in the work on ^{152}Sm [55], where, built on the first excited 0^+ state, a second $K = 0$ octupole band was observed. Given the strong evidence for shape coexistence in the nuclei under consideration, it is likely that a second octupole excitation built upon the coexisting structure of the excited states will be observed. Yet, the microscopic composition of the wave function and, consequently, the g-factor of this excited state must be different. Hence, the coexisting octupole excitation is expected to decay to the first excited octupole state by a comparably strong $M1$ transition. Thus, in nuclei which exhibit shape coexistence, the strong $M1$ transition to the first 3^-_1 level does not represent the unique fingerprint of an octupole-isovector excitation.

6 Summary

In this contribution, the ESPE of the spherical shells for the $N = 50$–56 Zr and Mo isotopes were extracted. The extracted trends of the ESPEs highlight two features which are important for the octupole excitations in this mass region: first, while for the Zr isotopes the $\nu 1h_{11/2}$ subshell migrates away from the other subshells with increasing filling of the $\nu 2d_{5/2}$ subshell, this is not the case for the Mo isotopes. Furthermore, for the Mo isotopes the $\nu 2d_{5/2}$ subshell migrates towards the other neutron subshells with increasing filling and the subshell gap closes, while this subshell gap remains preserved for the Zr isotopes. With respect to the first octupole excitations, their almost identical behaviour led to the conclusion that a type-II shape coexistence mechanism is at work. The presence of the proton $\pi 1g_{9/2}$ subshell in the $\pi[1g_{9/2}, 2p^{-1}_{3/2}]$ and $\pi[1g_{9/2}, 1f^{-1}_{5/2}]$ configurations alters the sequence of the neutron subshells in Zr isotopes towards a sequence resembling the one observed for the Mo isotopes. Concerning the proposed candidates for low-lying isovector octupole excitations in these Zr and Mo nuclei, the presented estimation of two-quasiparticle energies raises doubts. The basis states are found at too high energies in order to fulfil a simple state-mixing picture.

The members of the UWS group acknowledge financial support by the UK Science and Technology Facilities Council (STFC). MT and VW acknowledge financial support by the Deutsche Forschungsgemeinschaft (Grants Kr1796/2-1 and SFB-1245). Fruitful discussions with D. Tarpanov, C. Stoyanov, N. Pietralla, and N. Arsenev are gratefully acknowledged.

Appendix A.

In tables 7, 8, 9, 10 of this appendix the information about the employed experimental levels and their spectroscopic factors S or the product C^2S is given. Additionally the employed reactions these levels were measured with and the references where the data were published are provided.

Table 7. Levels in yttrium isotopes used to calculate the effective single-particle energies of proton subshells shown in table 2 and fig. 3. No C^2S value was given for the 1090 keV state in ^{95}Y. Additionally, the evaluted reactions and the data sets are given. All energies are given in keV.

Nucleus	$1g_{9/2+}$		$2p_{1/2-}$		$1f_{5/2-}$		$2p_{3/2-}$		Reaction and reference
	E	C^2S or S	E	C^2S or S	E	C^2S or S	E	C^2S or S	
^{89}Y	910	6.34	0	0.72	−1745	2.77	−1507	1.86	^{90}Zr$(e,e'p)$ [56];
	2610	0.41			−5040	0.29	−4000	0.12	^{88}Sr(d,n) [57]
^{91}Y	550	1.09	0	1.33	−922	1.5	−653	0.84	^{92}Zr$(d,{}^3\mathrm{He})$; [58];
			−2569	0.37	−1552	5.28	−1481	1.9	^{92}Zr(t,α) [59]
					−1974	0.21	−2475	0.38	
					−2205	1.21			
^{93}Y	775	0.81	0	1.58	−890	1.7	−599	0.89	^{94}Zr$(d,{}^3\mathrm{He})$ [58]
			−1280	1.51	−1280	4	−2530	0.5	
^{95}Y	1090		0	2.7	−827	9.9	−686	2.4	^{96}Zr$(d,{}^3\mathrm{He})$; [58];
					−1887	2.5	−2041	2.2	^{96}Zr$(\boldsymbol{t},\alpha)$ [60]

Table 8. Levels in niobium isotopes used to calculate the effective single-particle energies of proton subshells shown in table 2 and fig. 3. Additionally, the evaluted reactions and the data sets are given. All energies are given in keV.

Nucleus	$1g_{9/2+}$		$2p_{1/2-}$		$1f_{5/2-}$		$2p_{3/2-}$		Reaction and reference
	E	C^2S or S	E	C^2S or S	E	C^2S or S	E	C^2S or S	
^{91}Nb	0	2.6	−100	1.66	−1181	0.55	−1306	1.15	^{90}Zr$({}^3\mathrm{He},d)$ [37];
					−1842	4	−1606	2.35	^{92}Mo(t,α) [61]
^{93}Nb	0	7.9	−30	1.6	−1320	3.5	−680	1.2	^{92}Zr$({}^3\mathrm{He},d)$ [62,63];
	1080	0.4					−1320	1.9	^{94}Mo$(d,{}^3\mathrm{He})$ [64]
^{95}Nb	0	2.9	−237	1.7	−1021	2.6	−807	1.8	^{96}Mo$(\boldsymbol{t},\alpha)$ [60]
			−2383	0.13	−1273	4.4	−1215	1.8	
			−2486	0.27	−1662	0.38	−1589	0.16	
					−2302	0.82	−2768	0.12	
					−2599	0.31			
					−2670	0.42			
					−2724	0.47			
^{97}Nb	0	2.2	−737	2.1	−1435	5.2	−1247	2.6	^{96}Zr$({}^3\mathrm{He},d)$ [65];
	1160	1.2			−2113	1.2	−1761	0.24	^{98}Mo$(\boldsymbol{t},\alpha)$ [60]
	1945	0.09			−2541	1	−2047	0.07	
							−2388	0.34	

Table 9. Levels in zirconium isotopes used to calculate the effective single-particle energies of neutron subshells shown in table 3 and fig. 4. Additionally, the evaluted reactions and the data sets are given. All energies are given in keV.

Nucleus	$d_{5/2^+}$		$s_{1/2^+}$		$g_{7/2^+}$		$d_{3/2^+}$		$h_{11/2^-}$		Reaction and reference
	E	C^2S or S	E	C^2S or S	E	C^2S or S	E	C^2S or S	E	C^2S or S	
^{91}Zr	0	1.05	1212	0.83	1877	0.078	2048	0.63	2171	0.4	^{90}Zr(d,p);
	1476	0.018	2559	0.24	2203	0.34	2875	0.21	2333	0.048	^{90}Zr$(\alpha,{}^3$He) [66]
	6850	0.019	3330	0.01	3475	0.28	3087	0.12			
					3558	0.072	3291	0.15			
					3917	0.21	3682	0.1			
					4018	0.036					
^{93}Zr	0	3.84	942	1.84	2075	0.58	272	0.016	2363	0.132	^{92}Zr(d,p);
			1018	0.26			2770	1.08			^{92}Zr$(\alpha,{}^3$He) [67]
			1151	0.04							
			1222	0.012							
			1896	0.46							
			2100	0.14							
			2391	0.008							
			3077	0.036							
^{95}Zr	0	2.3	954	0.99	1619	0.48	1324	0.044	2022	0.13	^{94}Zr(d,p) [67,68];
			3300	0.109	2450	0.0101	1618	0.54	2625	0.155	^{94}Zr$(\alpha,{}^3$He) [67]
			3960	0.083	2724	0.312	1722	0.06	2834	0.046	
					4068	0.03	1892	0.084	3117	0.033	
							2291	0.148	3330	0.101	
							2376	0.144	3420	0.033	
							2625	0.05	3662	0.047	
							2834	0.12			
							2996	0.044			
							3062	0.132			
							3205	0.027			
							3528	0.088			
^{97}Zr	−1399	0.091	0	1.06	1265	1.05	1108	1.22	2265	0.56	^{96}Zr(d,p);
									3731	0.13	^{96}Zr$(\alpha,{}^3$He) [67]

Table 10. Levels in molybdenum isotopes used to calculate the effective single-particle energies of neutron subshells shown in table 3 and fig. 4. Additionally, the evaluted reactions and the data sets are given. All energies are given in keV.

Nucleus	$d_{5/2^+}$		$s_{1/2^+}$		$g_{7/2^+}$		$d_{3/2^+}$		$h_{11/2^-}$		Reaction and reference
	E	C^2S or S	E	C^2S or S	E	C^2S or S	E	C^2S or S	E	C^2S or S	
^{93}Mo	0	0.73	943	0.53	1365	0.27	1493	0.36	2311	0.45	^{92}Mo(d,p);
	1698	0.073	2442	0.071	1525	0.33	2179	0.036	3385	0.038	^{92}Mo$(\alpha,{}^3$He) [66]
	2144	0.004	2705	0.33	3023	0.04	2838	0.026	3529	0.018	
	2399	0.02			3210	0.056					
					3880	0.085					
					4000	0.25					
^{95}Mo	0	0.59	782	0.37	762	0.18	202	0.019	1932	0.26	^{94}Mo(d,p) [69]
	1963	0.08	1035	0.19	2118	0.11	1364	0.03			
			1299	0.004			1420	0.026			
			1692	0.006			1615	0.15			
			2049	0.097			2042	0.1			
			2357	0.058			2089	0.055			
			2595	0.055			2169	0.12			
			3056	0.019			2244	0.05			
							2383	0.036			
							2396	0.04			
							2830	0.036			
							2843	0.024			
							3037	0.15			
^{97}Mo	0	1.33	680	0.94	659	5.8	482	0.034	1437	3.35	^{96}Mo(d,p) [34];
	720	1.07	795	0.012	1024	0.9	1265	1.08	2429	1.04	^{98}Mo(p,d) [35];
	1286	0.25	889	0.042	1629	0.76	1516	0.095			^{98}Mo$(\boldsymbol{d},t)$ [36]
	1564	0.39	1550	0.16	1763	0.56	2152	1.02			
	1956	0.026	2034	0.23	1789	0.56	2315	0.11			
	2378	0.18	2462	0.086	2539	0.92					
	2419	0.06	2557	0.082							
			3154	0.081							
^{99}Mo	98	0.21	0	0.67	236	0.42	353	0.11	688	0.14	^{98}Mo(d,p) [69]
	619	0.02	529	0.04			552	0.43			
			896	0.02			896	0.09			
			1261	0.01							

References

1. F. Iachello, Phys. Rev. Lett. **53**, 1427 (1984).
2. F. Iachello, A. Arima, *The Interacting Boson Model* (Cambridge University Press, Cambridge, England, 1987).
3. K. Heyde, J. Sau, Phys. Rev. C **33**, 1050 (1986).
4. D. Bohle *et al.*, Phys. Lett. B **137**, 27 (1984).
5. W.D. Hamilton, A. Irback, J.P. Elliott, Phys. Rev. Lett. **53**, 2469 (1984).
6. G. Molnar, R.A. Gatenby, S.W. Yates, Phys. Rev. C **37**, 898 (1988).
7. U. Kneissl, N. Pietralla, A. Zilges, J. Phys. G **32**, R217 (2006).
8. N. Pietralla, P. von Brentano, A.F. Lisetskiy, Prog. Part. Nucl. Phys. **60**, 225 (2008).
9. K. Heyde, P. von Neumann Cosel, A. Richter, Rev. Mod. Phys. **82**, 2365 (2010).
10. K. Heyde, J.L. Wood, Rev. Mod. Phys. **83**, 1467 (2011).
11. S. Raman, C.W. Nestor, P. Tikkanen, At. Data Nucl. Data Tables **78**, 1 (2001).
12. `www.nndc.bnl.gov/endsf`.
13. `www.nndc.bnl.gov/xundl`.
14. G. Jacob *et al.*, Phys. Lett. B **468**, 13 (1999).

15. G. Kumbartzki *et al.*, Phys. Lett. B **562**, 193 (2003).
16. P. Mantica *et al.*, Phys. Rev. C **63**, 034312 (2001).
17. A. Chakraborty *et al.*, Phys. Rev. Lett. **110**, 022504 (2013).
18. T. Thomas *et al.*, Phys. Rev. C **88**, 044305 (2013).
19. T. Thomas *et al.*, Nucl. Phys. A **947**, 203 (2016).
20. C. Kremer *et al.*, arXiv:1606.09057v1.
21. T. Kibédi, R.H. Spears, At. Data Nucl. Data Tables **80**, 35 (2002).
22. L.P. Gaffney *et al.*, Nature **497**, 199 (2013).
23. H.J. Wollersheim *et al.*, Nucl. Phys. A **556**, 261 (1993).
24. P.A. Butler, W. Nazarejewicz, Rev. Mod. Phys. **68**, 349 (1996).
25. M. Scheck *et al.*, Phys. Rev. C **81**, 064305 (2010).
26. A. Hennig *et al.*, Phys. Rev. C **90**, 051302 (2014).
27. M. Scheck, J. Phys.: Conf. Ser. **366**, 012040 (2011).
28. C. Walz, Master Thesis, TU Darmstadt (2010) unpublished.
29. C. Walz, PhD Thesis, TU Darmstadt (2014) unpublished.
30. P. Singh *et al.*, Nucl. Phys. A **458**, 1 (1986).
31. S. Sen *et al.*, Nucl. Phys. A **537**, 100 (1992).
32. E.R. Flynn, D.D. Armstrong, J.G. Beery, Phys. Rev. C **1**, 703 (1970).
33. C. Fransen *et al.*, Phys. Rev. C **71**, 054304 (2005).
34. L.R. Medsker, H.E. Jackson, Phys. Rev. C **9**, 709 (1974).
35. P.K. Bindal *et al.*, Phys. Rev. C **12**, 390 (1975).
36. S.E. Vigdor, W. Haeberli, Nucl. Phys. A **253**, 55 (1975).
37. K.T. Knöpfle *et al.*, Nucl. Phys. A **159**, 642 (1970).
38. A. Bohr, B.R. Mottelson, *Nuclear Structure*, Vol. **I** (W. A. Benjamin Inc., New York, Amsterdam, 1969).
39. M. Wang *et al.*, Chin. Phys. C **36**, 1603 (2012).
40. R. Schwengner *et al.*, Phys. Rev. C **78**, 064314 (2008).
41. C. Fransen *et al.*, Phys. Rev. C **70**, 044317 (2004).
42. V. Werner *et al.*, Phys. Lett. B **550**, 140 (2002).
43. C. Fransen *et al.*, Phys. Rev. C **67**, 024307 (2003).
44. M. Zweidinger *et al.*, in preparation.
45. G. Rusev *et al.*, Phys. Rev. Lett. **95**, 062501 (2005).
46. G. Rusev *et al.*, Phys. Rev. C **73**, 044308 (2006).
47. P. Garrett *et al.*, Phys. Rev. C **68**, 024312 (2003).
48. J.P. Schiffer, W.W. True, Rev. Mod. Phys. **48**, 191 (1976).
49. A. de-Shalit, I. Talmi, *Nuclear Shell Theory* (Dover Publications, Mineola, 2004).
50. K. Heyde, *The Nuclear Shell Model* (Springer Verlag, Berlin, 1990).
51. R.F. Casten, *Nuclear Structure from a Simple Perspective* (Oxford University Press, Oxford, 2005).
52. Y. Tsunoda *et al.*, Phys. Rev. C **89**, 031301 (2014).
53. B.J. Lund *et al.*, Phys. Rev. C **51**, 635 (1995).
54. C. Walz *et al.*, Phys. Rev. Lett. **106**, 062501 (2011).
55. P. Garrett *et al.*, Phys. Rev. Lett. **103**, 062501 (2009).
56. J.W.A. den Herder *et al.*, Nucl. Phys. A **490**, 507 (1988).
57. J.L. Horton, C.E. Hollandsworth, Phys. Rev. C **13**, 2212 (1976).
58. B.M. Preedom, E. Newman, J.C. Hiebert, Phys. Rev. **166**, 1156 (1968).
59. J.C. Hardy, W.G. Davies, W. Darcey, Nucl. Phys. A **121**, 103 (1968).
60. E.R. Flynn *et al.*, Phys. Rev. C **28**, 575 (1983).
61. R. Chapman, J.E. Kitching, W. McLatchie, Nucl. Phys. A **196**, 347 (1972).
62. M.R. Cates, J.B. Ball, E. Newman, Phys. Rev. **187**, 1682 (1969).
63. G. Finkel *et al.*, Nucl. Phys. A **217**, 197 (1973).
64. H. Ohnuma, J.L. Yntema, Phys. Rev. **176**, 1416 (1968).
65. L.R. Medsker, Phys. Rev. C **8**, 1906 (1973).
66. D.K. Sharp *et al.*, Phys. Rev. C **87**, 014312 (2013).
67. C.R. Bingham, G.T. Fabian, Phys. Rev. C **7**, 1509 (1973).
68. K. Sonnabend *et al.*, Phys. Rev. C **68**, 048802 (2003).
69. J.B. Moorhead, R.A. Moyer, Phys. Rev. **184**, 1205 (1969).